Surface & Coatings Technology 292 (2016) 37–43

Contents lists available at ScienceDirect

Surface & Coatings Technology

journal homepage: www.elsevier.com/locate/surfcoat

Nanocrystalline Co-Ni alloy coating produced with supercritical carbon dioxide assisted electrodeposition with excellent wear and corrosion resistance

Cansen Liu, Fenghua Su *, Jizhao Liang

School of Mechanical and Automotive Engineering, South China University of Technology, Guangzhou 510640, China

ARTICLE INFO

Article history:
Received 21 December 2015
Revised 2 March 2016
Accepted in revised form 8 March 2016
Available online 10 March 2016

Keywords:
Cobalt-Nickel alloy
Supercritical carbon dioxide
Electrodeposition
Wear
Corrosion

ABSTRACT

Co-Ni alloy coatings were produced by two different electrodeposition techniques, i.e., supercritical carbon dioxide (Sc-CO_2) assisted electrodeposition and conventional electrodeposition in air. Effect of the two electrodeposition techniques on surface morphology, grain size, crystalline texture, microhardness, wear and corrosion resistance of the resulting Co-Ni alloy coatings were investigated. The results show that the Co-Ni alloy coating electroplated with the aid of Sc-CO_2 fluid exhibits brighter surface appearance, lower surface roughness and smaller grain size. The preferred orientation plane of (1 0 0) for the coating prepared in air is changed to be close-packed (1 1 1) facets for the coating produced in emulsified Sc-CO_2 bath. The microhardness of the Co-Ni alloy coating deposited in emulsified Sc-CO_2 bath is much higher than that of the one produced by the traditional electrodeposition. Moreover, the Co-Ni alloy coating produced in emulsified Sc-CO_2 bath possesses better wear and corrosion resistance, which wear and corrosion rate are respectively about one fourth and half of the one deposited by the conventional electrodeposition. This work offers an attractive strategy for fabricating Co-Ni alloy coating as protective layers to increase the lifetime of components exposed to corrosion and wear condition.

1. Introduction

Surface coatings or deposits are often used as protective layers to increase the lifetime of components exposed to corrosion and wear condition [1–5]. Due to the low cost and easy control, electrodeposition is recognized as a technologically feasible and economically superior technique for producing coatings to improve appearance of surfaces, to give good corrosion protection and to improve wear resistance of the substrate [6–12]. Many reports proved that the coating with nanocrystalline structure exhibits higher hardness, better wear and corrosion resistances than the one with microcrystalline structure [13–16]. However, to produce coatings with nanocrystalline structure, the over potential must be very high, resulting in severe hydrogen (H_2) evolution reaction during the plating process. H_2 gas bubbles formed on the surface of cathode caused defects on the electrodeposited materials, resulting in bad corrosion and wear properties of the coating [17].

Carbon dioxide (CO_2) is non-polar, solubility of H_2 is high in CO_2 [18, 19]. Desorption of H_2 gas bubbles from the surface of cathode could be significantly enhanced in supercritical carbon dioxide (Sc-CO_2). The application of Sc-CO_2 in electrodeposition process is believed to solve the hydrogen evolution problem. Additionally, CO_2 is nontoxic, nonflammable, abundant and cheap. The critical point of Sc-CO_2 is relatively low when compared to the other solvents. Therefore, the application of Sc-CO_2 in electroplating reaction is attractive as well as advantageous. However, metal salts are generally soluble in water, but water and CO_2 are almost not miscible [20]. Because of this, pure Sc-CO_2 is not suitable for electroplating. This problem can be solved by the emulsification of Sc-CO_2 with the addition of surfactant [21–23]. In recent years, a number of works were done to produce Nickel (Ni) coating with excellent properties using Sc-CO_2 as reaction medium [24–28]. Chung et al. [24] prepared Ni coating at atmospheric pressure and in supercritical CO_2 fluid. They found that the Ni coating electroplated in the latter case exhibited lower surface roughness and higher hardness. Chang et al. [25] reported that bright Ni coating can be obtained without usage of brightener when supercritical carbon dioxide emulsion (Sc-CO_2-E) is used. They also confirmed that the grain size of Ni coating electroplated with Sc-CO_2-E was finer than that of the coating produced by conventional electrodeposition. Rahman et al. [26] investigated the microstructure and wear behavior of Ni coatings electrodeposited in conventional electroplating system and in Sc-CO_2-E. The results showed that the Ni coatings electroplated in the latter case had higher uniformity, smaller grain size, higher Vickers hardness, and better wear resistance.

When compared to Ni deposits, Co-Ni alloy deposits exhibit better wear and corrosion resistance. In addition, nanocrystalline Co-Ni alloy coatings have potential to be used in aerospace, automobile and general industries as an alternative to hard chromium coatings due to the high hardness, excellent wear and corrosion resistance [29–31]. Unfortunately,

* Corresponding author.
E-mail address: fhsu@scut.edu.cn (F. Su).

http://dx.doi.org/10.1016/j.surfcoat.2016.03.027
0257-8972/

synthesis and characterizations of Co-Ni alloy coating produced by Sc-CO_2 assisted electrodeposition were not reported till now. In this work, the Co-Ni alloy coatings are produced by Sc-CO_2 assisted electrodeposition and conventional electrodeposition at atmospheric pressure, respectively. The microstructure and properties of the electroplated Co-Ni alloy coatings are studied profoundly. The inherent relationships between the electroplating techniques, the microstructures, and the properties of the resulting Co-Ni alloy coatings are well established.

2. Experimental

2.1. Electrodeposition of the Co-Ni alloy coatings

A high pressure experimental apparatus is used for electroplating reaction. Schematic of the Sc-CO_2 assisted deposition system is shown in Fig. 1. The high pressure reaction vessel is 150 mL stainless steel that is incorporated with a stirrer and temperature control system. A Co plate (purity 99.9%) and a brass plate with size of 20 × 40 mm^2 are used as the anode and working cathode, respectively. Distance between the cathode and anode is kept at 20 mm. Prior to plating, the surface of the brass plates are mechanically polished using abrasive water paper from 600 to 1500 grade and sequentially cleaned ultrasonically in distilled water and acetone to remove contaminations on the substrate surface. The bath compositions and the operational parameters for electrodepositing Co-Ni alloy coating are given in Table 1. The surfactant used is polyoxyethylene lauryl ether (CAS No. 9002-92-0). Two types of electrodeposition baths, namely conventional and emulsified sc-CO_2, are used in this investigation. For conventional electroplating, specimens are prepared at ambient pressure and 50 °C in the conventional aqueous electrolyte without addition of surfactant. The emulsified Sc-CO_2 bath is prepared by purging pressurized CO_2 at 10 MPa into the conventional aqueous electrolyte with addition of surfactant to ensure an emulsified fluid obtained. The bath consists of 100 mL of conventional aqueous electrolyte and 50 mL Sc-CO_2 fluid. The electrodeposition is conducted using an Intelligent Multiwave Electroplating Equipment supplied by Handan Dashun Electroplating Equipment Co., Ltd., in China. The Co-Ni alloy coatings produced by conventional deposition and Sc-CO_2 assisted deposition are dubbed as Co-Ni-I and Co-Ni-II, respectively.

2.2. Characterizations of the Co-Ni alloy coatings

The morphologies of the Co-Ni alloy coatings surface were analyzed using a Quanta 200 scanning electron microscopy (SEM) and a CSPM4000 atomic force microscopy (AFM). The element compositions of the Co-Ni alloy coating was measured by energy dispersive X-ray spectroscopy (EDS) microanalyzer attached with the Quanta 200 SEM. The crystal structures of the as-plated coatings were studied using a Philips X'pert X-ray diffractometer (XRD, Cu-Kα radiation) operating at 40 kV and 40 mA over the 2 θ range 5–80°. The microhardness was measured on a Vicker's microhardness tester with a load of 100 g applied for 10 s. Eight measurements were made on surface for a sample and the average was reported.

Table 1
Bath compositions and operational parameters for electrodepositing Co-Ni alloy coating.

Component/deposition condition	Concentration/value
Cobalt sulfate	30 $g \cdot L^{-1}$
Nickel sulfate	100 $g \cdot L^{-1}$
Sodium chloride	30 $g \cdot L^{-1}$
Boric acid	30 $g \cdot L^{-1}$
Lauryl sodium sulfate	0.1 $g \cdot L^{-1}$
Saccharin sodium	1.0 $g \cdot L^{-1}$
Surfactant	1.0 vol%
Dense carbon dioxide (minimum purity of 99.9%)	50 mL
pH	5.0
Temperature	50 °C
Current density	2.5 $A \cdot dm^{-2}$
Agitating speed	450 rpm
Deposition time	30 min
Pressure	10 MPa

The friction and wear behaviors of the Co-Ni alloy coatings sliding against GCr15 steel ball with diameter of 4.0 mm were tested on a ball-on-disk tribometer under dry sliding conditions, room temperature and ambient humidity. The tests were performed under sliding speed of 0.188 ms^{-1} and load of 2.0 N for 10 min. The diameters of wear tracks on coatings were 12.0 mm. After the wear tests, three-dimensional (3D) profiles of the wear tracks were measured using a Talysurf CLI 1000 surface profile measurement system to achieve the wear volume. The wear rates of all the coatings were calculated from $K = V/S \cdot F$, where V is the wear volume (mm^3), S the total sliding distance (m) and F the normal load (N). Three replicate friction and wear tests were carried out for each specimen and the average was reported with their errors. After sliding, the wear surfaces of the coatings were analyzed using the Quanta 200 SEM.

Electrochemical corrosion test was carried out in a three electrode cell. A platinum plate and saturated silver/silver chloride (Ag/AgCl) electrode were used as the counter and reference electrode, respectively. The as-fabricated Co-Ni alloy coatings were used as the working electrode. Measurements were performed by an electrochemical workstation (CorrTest CS310, Wuhan Corr Test Instrument Co. Ltd., China) at room temperature with neutral 3.5 wt.% NaCl solution as corrosive medium. Before electrochemical tests, samples were mounted using paraffin wax with surface area of 1 cm^2 exposed to the corrosive medium. All the samples were immersed for 30 min, allowing the system to be stabilized before the potentiodynamic polarization and electrochemical impedance spectroscopy (EIS) tests. The potentiodynamic polarization curves were recorded at a sweep rate of 0.5 mVs^{-1} from −200 to 200 mV versus the open circuit potential. As to EIS measurements, the employed amplitude of the sinusoidal signal was 10 mV, and the frequency range studied was from 10^5 to 10^{-2} Hz. The average value from three replicates for each kind of specimen was reported.

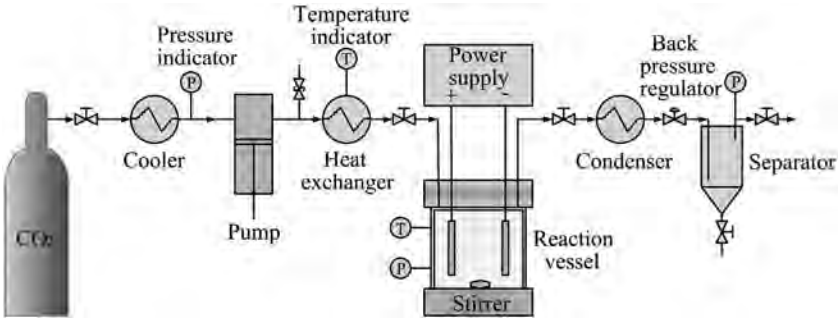

Fig. 1. Schematic of the Sc-CO_2 assisted electrodeposition system for fabricating Co-Ni alloy coating.

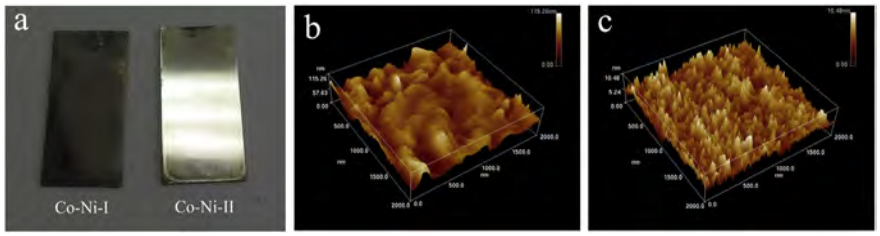

Fig. 2. Surface appearance (a) and AFM images ((b) Co-Ni-I; (c) Co-Ni-II) of the Co-Ni alloy coatings electroplated by different techniques.

3. Results and discussion

3.1. Morphology, microstructure and hardness of the Co-Ni alloy coatings

Fig. 2a shows the surface appearance of the two Co-Ni alloy coatings produced by traditional electrodeposition and Sc-CO_2 assisted electrodeposition. The surface appearance of the Co-Ni alloy coating produced by the conventional electrodeposition (Co-Ni-I) is dim. However, the Co-Ni coating electroplated in emulsified Sc-CO_2 bath (Co-Ni-II) displays noticeably brighter and smoother surface appearance than the Co-Ni-I coating. AFM images of the Co-Ni-I and Co-Ni-II alloy coatings are shown in Fig. 2b and c, respectively. As shown in Fig. 2b, the Co-Ni-I coating surface displays coarse columnar crystal structure with high surface roughness. In the case of Co-Ni-II coating (Fig. 2c), the surface displays lower surface roughness and the surface morphology is featured with finer and dense columnar crystal structure. The surface roughness measured by surface profile measurement system shows that the average surface roughness of the Co-Ni-II coating is approximately one third of the Co-Ni-I coating.

SEM images of surface and cross-section for the Co-Ni alloy coatings electroplated by the two different techniques are shown in Fig. 3. It is clear that the surface morphologies of the alloy coatings are greatly affected by the electrodeposition method used. The Co-Ni-I coating exhibits a rough surface that is characterized with wheat-like structure (Fig. 3a and b). In contrast with the Co-Ni-I coating, the Co-Ni-II coating (Fig. 3d and e) shows a compact and smooth surface. EDS analysis show that the Co content in the Co-Ni-II coating is slightly higher than that in the Co-Ni-I coating (Table 2). It is also note that the percentage of Co in the alloy coatings is higher than that in the electrolyte in agreement with other reports [29,32], which might be attributed to the anomalous co-deposition of Co-Ni alloy. Bai et al. [32] thought the anomalous deposition resulting from the higher adsorption ability of $Co(OH)^+$ than $Ni(OH)^+$ on the cathode surface. The deposition of Co is promoted by the surface enrichment of adsorbed metal hydroxide cations. Therefore, Co content in the coating is always higher than that in the electrolyte.

The cross-sectional SEM images of the two different Co-Ni alloy coatings are respectively shown in Fig. 3c and f. It is obvious that the thickness 11.5 μm of the Co-Ni-II alloy coating is thinner than that for the Co-Ni-I alloy coating (15.0 μm), which suggests that the deposition rate in the emulsified Sc-CO_2 bath is lower than that in the conventional bath. The finding agrees well with other reports previously [33–36]. In the emulsified Sc-CO_2 bath, the formation of micelle caused a reduction in the number of active sites at the substrate/electrolyte interface for electrochemical reaction [25]. As a result, the deposition rate is hindered and the thickness of the corresponding coating is thinner. The lower conductivity of the emulsified Sc-CO_2 bath is also responsible for the thinner coating [37]. Carbonic acid is formed when CO_2 is dissolved in water, which increases the concentration of H^+ in electrolyte. During electrodeposition, the rapid reduction of increased amounts of H^+ ions to H_2 causes a lower current efficiency [38]. Meanwhile, it can be seen from Fig. 3c that the Co-Ni-I coating has a number of pinholes (black circle in Fig. 3c). The pinholes produced by hydrogen reduction are commonly accompanied with metal ion reduction during electroplating. Hydrogen bubbles formed near cathode will absorb onto the surface of cathode and forms pinholes in the coating electroplated. The solubility of H_2 in liquid phase can be enhanced by the introduction of Sc-CO_2 [39,40]. The increase of H_2 solubility in Sc-CO_2 reduces bubble formation on the deposit coating and thereby minimizes pinhole formation. As a result, no pinholes are observed in the Co-Ni alloy coating produced in the presence of Sc-CO_2 (Fig. 3f).

XRD patterns of the Co-Ni alloy coatings fabricated by different electrodeposition techniques are shown in Fig. 4. It is clear that the Co-Ni-I coating displays a strong (1 0 0) peak and a relatively strong (2 2 0) peak. In contrast, the Co-Ni-II coating exhibits a weak (1 0 0) peak and a strong new (1 1 1) peak. In addition, the sings of peak broadenings are observed for the Co-Ni-II coating, indicating this coating has smaller grain size [41]. Table 3 shows the average grain size calculated using the Scherrer's equation [42] and the microhardness for the two different Co-Ni alloy coatings. It can be seen that the two Co-Ni alloy coatings are nanocrystalline structure, irrespective of

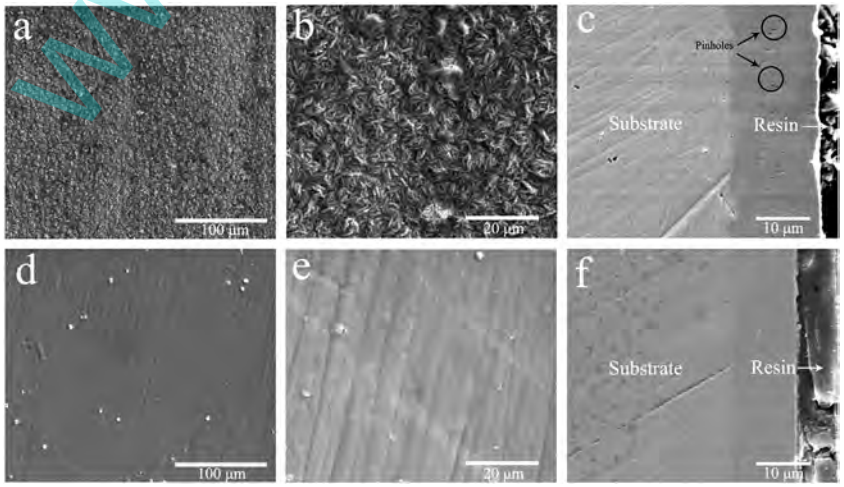

Fig. 3. SEM images of the surface and cross-section for the Co-Ni alloy coatings electroplated by different techniques ((a)–(c) Co-Ni-I; (d)–(f) Co-Ni-II).

Table 2
Mass fractions of Co and Ni elements in the Co-Ni alloy coatings electroplated by different techniques.

Sample	Element and its mass fraction (wt.%)	
	Co	Ni
Co-Ni-I	73.66	26.34
Co-Ni-II	76.55	23.45

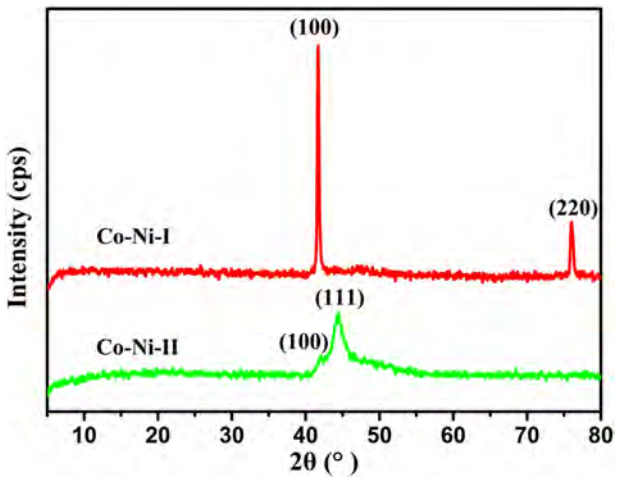

Fig. 4. XRD patterns of the Co-Ni coatings electroplated by different techniques.

Table 3
Average grain size and microhardness of the Co-Ni alloy coatings electroplated by different techniques.

Sample	Average grain size (nm)	Microhardness (kgf mm^{-2})
Co-Ni-I	40 ± 4	360 ± 15
Co-Ni-II	10 ± 2	600 ± 20

the electrodeposition techniques. The average grain size of the Co-Ni alloy coating deposited in emulsified Sc-CO_2 bath is about 10 nm, which is much smaller than that around 40 nm for the coating prepared in air. Generally, the microhardness of Co-Ni alloy coatings is in the range of 300–500 kgf mm^{-2} depending on the grain size and the cobalt content [30]. As shown in Table 3, the Co-Ni-II coating displays microhardness as high as 600 kgf mm^{-2} that is much higher than 360 kgf mm^{-2} for the Co-Ni-I coating. It suggests that Sc-CO_2 fluid assisted electrodeposition displays excellent ability in microhardness improvement.

The electroplating in emulsified Sc-CO_2 bath is found to have periodic plating characteristic that similar to pulse plating, where there is a reaction on and off time. When the electroplating solution comes in contact with the cathode, the new nucleus form and the crystal grows. The growth of crystal stops when Sc-CO_2 comes in contact with the cathode, because electrical conductivity and solubility of metal salts are low in Sc-CO_2 [25]. The preferred orientation of the crystal growth on electrodeposition is affected by electroplating conditions, i.e. electrolyte composition, temperature, pH, current density, stirring and organic additions [43,44]. The Co-Ni alloy coating produced by conventional electrodeposition in air displays (1 0 0) preferred orientation. In crystallization process, atoms incline to crystallization in the close-grained plane which has lower surface energy [45]. The atomic density of (1 0 0) plane is lower than that of (1 1 1) plane, hence the surface energy of (1 1 1) plane is lower than that of (1 0 0) plane. The growth of crystal stops when Sc-CO_2 comes in contact with the cathode means an off-time, which gives time to the atoms to migrate to the most stable position during the electrodeposition process. Therefore, more atoms rest on the (1 1 1) plane resulting in the Co-Ni-II coating exhibiting obvious (1 1 1) preferred orientation (Fig. 4). In addition, the formation of new nucleus during the on-time and the crystal growth stopping during the off-time leads to the grain refinement for the coating electroplated in emulsified Sc-CO_2 bath. The smaller grain size corresponds to the enhanced microhardness for the Co-Ni-II coating (Table. 3) according to the well-known Hall-Petch equation. Moreover, Sc-CO_2 fluid can effuse through solids like a gas, and dissolve materials like a liquid and has the interface tension between a liquid and a gas. Viscosity and surface tension of Sc-CO_2 are lower than those of the aqueous electrolyte. The lower viscosity of the reaction medium favors the mobility of the reactants in electrolyte, which can improve the nucleus density of the deposit during electrodeposition. Furthermore, desorption of H_2 bubbles from the surface of cathode are significantly enhanced in Sc-CO_2 due to the non-polarity of CO_2 molecular. H_2 bubbles are desorbed from the surface of cathode by dissolution in Sc-CO_2 during the off-time. The high nucleus density and enhancing desorption of H_2 gas bubbles from surface of cathode corresponds to the bright and smooth surface (Figs. 2 and 3) for the alloy coating produced by Sc-CO_2 assisted electrodeposition [25].

3.2. Wear and corrosion resistance of the Co-Ni alloy coatings

Fig. 5a shows the typical friction coefficient curves of the Co-Ni alloy coatings produced by the different electrodeposition techniques. It can be seen that the friction coefficient curves of the two Co-Ni alloy coatings increase to a certain value and maintained at this level until the end of the test. In contrast to the Co-Ni-I coating, the friction coefficient curve of the Co-Ni-II coating increases more slowly and steadily with the increase of sliding distance. The average friction coefficient and wear rate of the two different Co-Ni alloy coatings are shown in Fig. 5b. The Co-Ni-II coating exhibits lower average friction coefficient

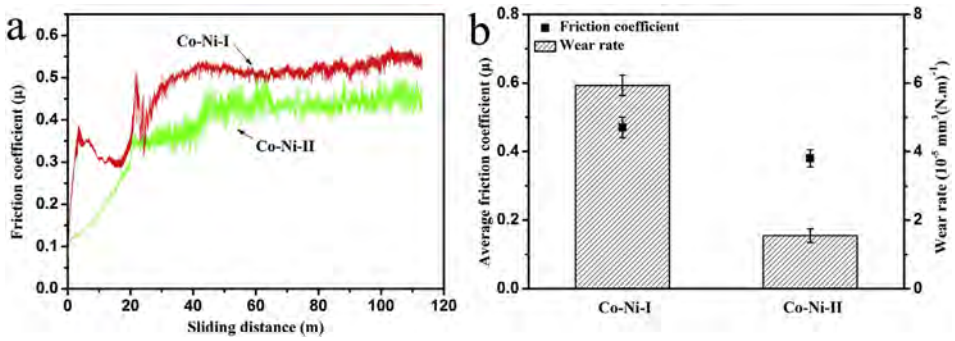

Fig. 5. Typical friction coefficient curves (a), average friction coefficient and wear rate (b) of the Co-Ni alloy coatings electroplated by different techniques.

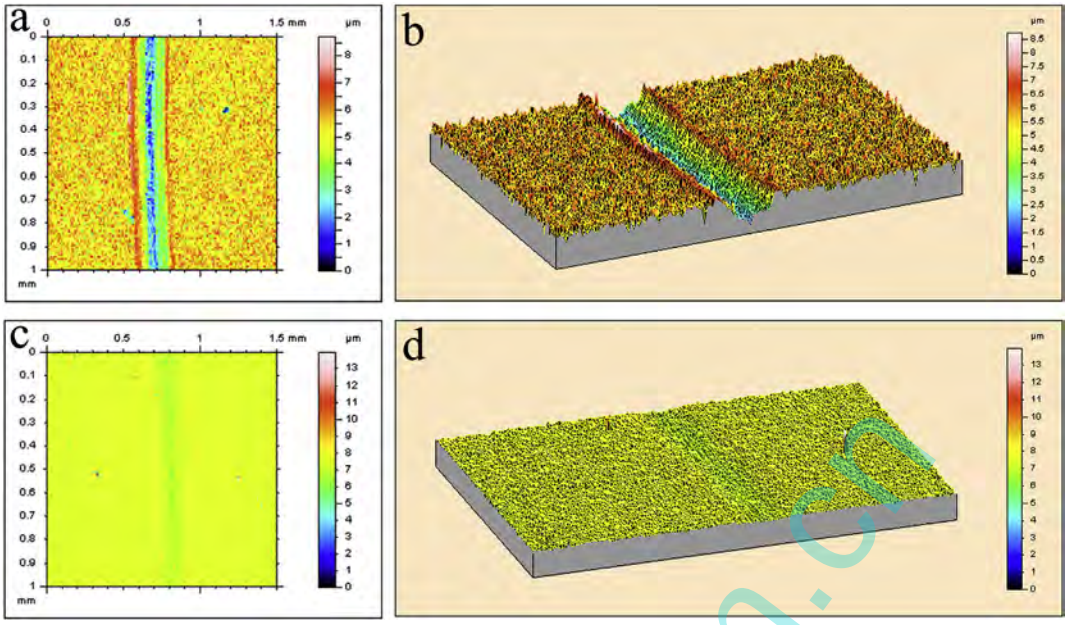

Fig. 6. Typical 3D topographies of the wear scar of the Co-Ni alloy coatings electroplated by different techniques ((a) and (b) Co-Ni-I; (c) and (d) Co-Ni-II).

and wear rate than the Co-Ni-I coating. The wear rate of the Co-Ni-II coating is about 1.55×10^{-5} $mm^3(N \cdot m)^{-1}$, which is much lower than that of 5.93×10^{-5} $mm^3(N \cdot m)^{-1}$ for the Co-Ni-I coating. The lower wear rate of the Co-Ni-II coating might be attributed to its higher microhardness (Table. 3). According to the classical Archard's law, the wear rate is proportional to the inverse microhardness of materials under the same wear conditions [29]. Apart from the microhardness, the phase structures of the two coatings also affect their wear resistances. As shown in Fig. 4, Co-Ni-II coating displays a strong close-packed (1 1 1) preferred orientation, which can avoid severe adhesive wear that happened during the rubbing process [45].

Typical 3D topographies of the wear scar of the Co-Ni alloy coatings electroplated by different techniques are shown in Fig. 6. It is obvious that the wear scar of the Co-Ni-I coating (Fig. 6a and b) is wider and deeper than that of the Co-Ni-II coating (Fig. 6c and d). The results indicate that the Co-Ni-II coating has experienced a slight wear but the Co-Ni-I coating has been severely destroyed by the counterpart balls during the rubbing process. The 3D topographies shown in Fig.6 agree well with the results shown in Fig. 5b. It is indeed that Sc-CO_2 assisted deposition can endow the produced Co-Ni coating with better wear resistance.

Fig. 7 shows the SEM images of the worn surfaces for the two Co-Ni alloy coatings. As shown in Fig. 7a and b, the worn surface of the Co-Ni-I

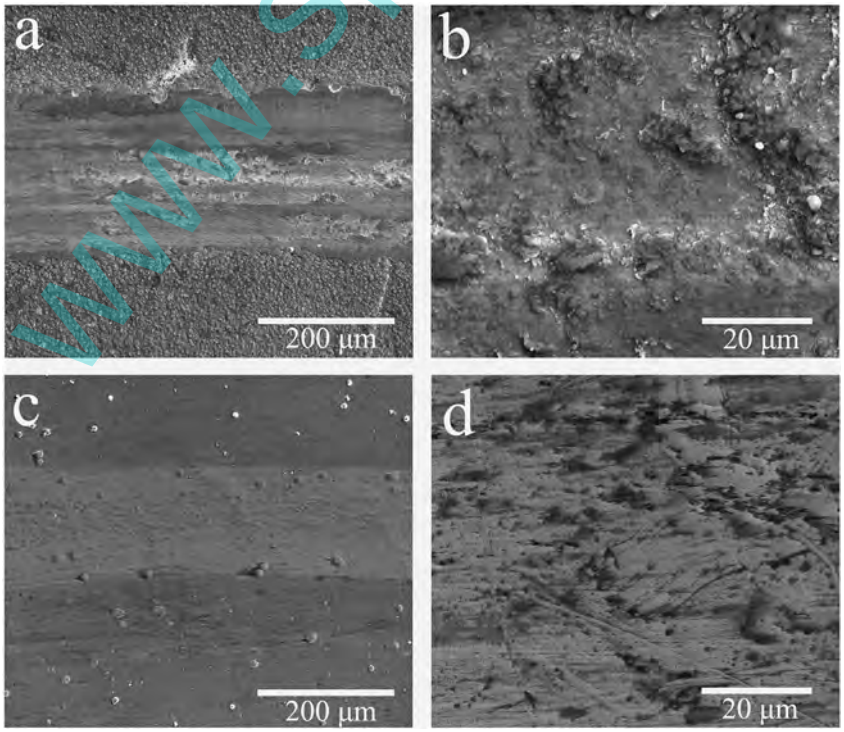

Fig. 7. SEM images of the worn surfaces of the Co-Ni alloy coatings electroplated by different techniques ((a) and (b) Co-Ni-I; (c) and (d) Co-Ni-II).

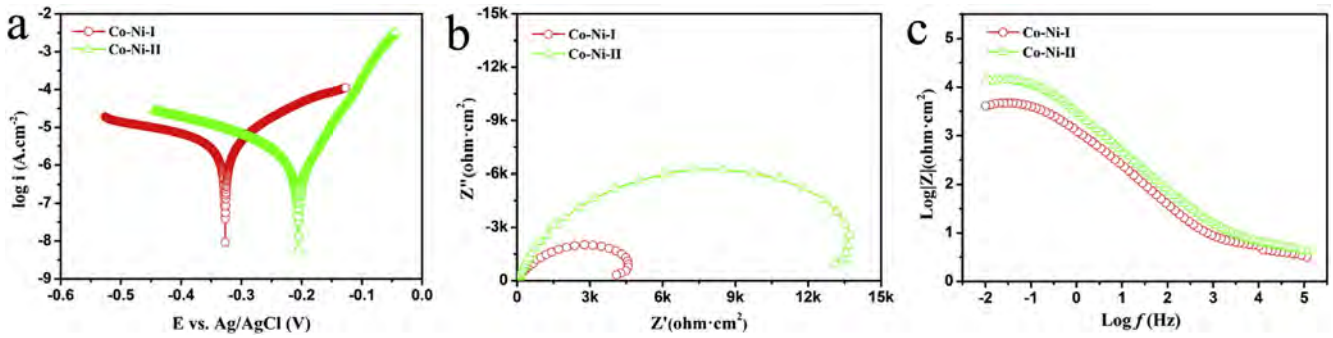

Fig. 8. Potentiodynamic polarization curves (a), Nyquist plots (b) and Bode plots (c) of the Co-Ni alloy coatings measured in 3.5 wt.% NaCl solution.

coating shows plastic deformation and severe wear features with delaminating structure, which might be attributed to the low hardness and rough surface of this coating (Fig. 3 and Table. 3). These results demonstrate that the severe adhesive wear has occurred during the rubbing process of the Co-Ni-I coating. The severe adhesive wear results in the wider and deeper wear scar (Fig. 6a and b). In the case of Co-Ni-II coating (Fig. 7c and d), the worn surface is featured with slight scratch without signs of severe plastic deformation and adhesion. The characterizations of the worn surfaces indicates a change in wear mechanism from severe adhesive wear for the Co-Ni-I coating to slight abrasive wear for the Co-Ni-II coating.

The potentiodynamic polarization curves of the two different Co-Ni alloy coatings measured in 3.5 wt.% NaCl solution are shown in Fig. 8a. The corrosion potential (E_{corr}), corrosion current density (i_{corr}) and corrosion rate that are calculated using the program CorShow from the potentiodynamic polarization curves are listed in Table 4. The E_{corr} of Co-Ni-II coating is above 100 mV more positive than Co-Ni-I coating. The i_{corr} of Co-Ni-II coating is less than half the value of Co-Ni-I coating. Moreover, the Co-Ni-II coating exhibits low corrosion rate, approximately 48% that of Co-Ni-I coating. These results confirms that the sample prepared in Sc-CO_2 fluid displays much better corrosion resistance than the one fabricated by conventional electrodeposition technique due to its more positive E_{corr}, lower i_{corr} and lower corrosion rate.

The Nyquist plots and Bode plots of Co-Ni alloy coatings measured in 3.5 wt.% NaCl solution are shown in Fig. 8b and c, respectively. The diameter of the capacitive loop in the Nyquist plots represents the polarization resistance of the work electrode. As shown in Fig. 8b, the Co-Ni-II coating exhibits an impedance value around $1.5 \times 10^4\ \Omega \cdot cm^2$ that is about three times higher than that of the Co-Ni-I coating. It is clear that the Co-Ni-II coating possesses a higher impedance modulus than the Co-Ni-I coating at low frequency, as shown in Fig. 8c. These results further confirm that the coating produced with the aid of Sc-CO_2 has better corrosion resistance than the one produce in air.

The better corrosion resistance of Co-Ni-II coating might be attributed to its smooth and compact surface (Figs. 2 and 3). A smoother surface means smaller area exposing to the attack of anodic dissolution, and the compact structure can prevent the corrosive medium (Cl^-) from eroding the coating or reaching the interface of coating and substrate. In addition, the average grain size has great influence on the electrochemical corrosion behavior of the nanocrystalline Co-Ni alloy coatings. The small grain size for a coating can provide much smaller cathode/anode surface ratio against localized corrosion due to the even distribution of corrosion current, which benefits the resistance to corrosion [14]. Therefore, it can be concluded that smaller grain size, smoother and compact surface corresponds to the improved corrosion resistance for the Co-Ni alloy coating produced with the aid of Sc-CO_2.

Table 4
Corrosion potential (E_{corr}), corrosion current density (i_{corr}) and corrosion rate of the Co-Ni alloy coatings measured in 3.5 wt.% NaCl solution.

Sample	E_{corr} (mV)	i_{corr} (A·cm^{-2})	Corrosion rate (mm·y^{-1})
Co-Ni-I	−327.7	2.45×10^{-6}	2.88×10^{-2}
Co-Ni-II	−206.1	1.17×10^{-6}	1.38×10^{-2}

4. Conclusions

A novel method of supercritical CO_2 assisted electrodeposition has been established to synthesize nanocrystalline Co-Ni alloy coating. The Co-Ni alloy coating prepared by Sc-CO_2 assisted electrodeposition exhibits smoother and brighter surface, smaller grain size and more compact microstructure than the one produced by conventional electrodeposition. The (1 0 0) preferred orientation for the Co-Ni alloy coating electroplated in air is changed to be (1 1 1) preferred orientation for the coating produced in emulsified Sc-CO_2 bath. Periodic plating characteristic, enhanced nucleus density and hydrogen desorption are believed to be the reasons for the change of morphologies and structures for the as-prepared Co-Ni alloy coating produced by Sc-CO_2 assisted electrodeposition. In addition, the introduction of Sc-CO_2 fluid during electrodeposition endows the as-prepared Co-Ni alloy coating with higher microhardness and better wear and corrosion resistance, which is related to the improved microstructure for this alloy coating.

Acknowledgments

The authors are grateful to the financial support of the National Natural Science Foundation of China (Grants: 51275176) and the Guangdong Natural Science Funds for Distinguished Young Scholar (2015A030306026).

References

[1] H. Ogihara, H. Wang, T. Saji, Electrodeposition of Ni-B/SiC composite films with high hardness and wear resistance, Appl. Surf. Sci. 296 (2014) 108–113.
[2] E. Correa, A.A. Zuleta, L. Guerra, M.A. Gómez, J.G. Castaño, F. Echeverría, H. Liu, P. Skeldon, G.E. Thompson, Tribological behavior of electroless Ni-B coatings on magnesium and AZ91D alloy, Wear 305 (2013) 115–123.
[3] S. Zhu, L. Chen, Y. Wu, Y. Hu, T. Liu, K. Tang, Q. Wei, Microstructure and corrosion resistance of Cr/Cr_2N multilayer film deposited on the surface of depleted uranium, Corros. Sci. 82 (2014) 420–425.
[4] C. Lee, Wear and corrosion behavior of electrodeposited nickel-carbon nanotube composite coatings on Ti-6Al-4V alloy in Hanks' solution, Tribol. Int. 55 (2012) 7–14.
[5] M. Costa, M. Cioffi, H.J.C. Voorwald, V. Guimaraes, An investigation on sliding wear behavior of PVD coatings, Tribol. Int. 43 (2010) 2196–2202.
[6] N. Imaz, M. Ostra, M. Vidal, J. Díez, M. Sarret, E. García-Lecina, Corrosion behaviour of chromium coatings obtained by direct and reverse pulse plating electrodeposition in NaCl aqueous solution, Corros. Sci. 78 (2014) 251–259.
[7] L. Lee, É. Régis, S. Descartes, R.R. Chromik, Fretting wear behavior of Zn–Ni alloy coatings, Wear 330 (2015) 112–121.
[8] F. Su, K. Yao, C. Liu, P. Huang, Rapid fabrication of corrosion resistant and superhydrophobic cobalt coating by a one-step electrodeposition, J. Electrochem. Soc. 160 (2013) D593–D599.
[9] Q. Liu, D. Chen, Z. Kang, One-step electrodeposition process to fabricate corrosion-resistant superhydrophobic surface on magnesium alloy, ACS Appl. Mater. Interfaces 7 (2015) 1859–1867.

[10] C. Liu, F. Su, J. Liang, Producing cobalt-graphene composite coating by pulse electrodeposition with excellent wear and corrosion resistance, Appl. Surf. Sci. 351 (2015) 889–896.
[11] M. Surender, B. Basu, R. Balasubramaniam, Wear characterization of electrodeposited Ni-WC composite coatings, Tribol. Int. 37 (2004) 743–749.
[12] A. Gajewska-Midziałek, B. Szeptycka, D. Derewnicka, A. Nakonieczny, Wear resistance of nanocrystalline composite NI-B coatings, Tribol. Int. 39 (2006) 763–768.
[13] N.P. Wasekar, P. Haridoss, S. Seshadri, G. Sundararajan, Sliding wear behavior of nanocrystalline nickel coatings: influence of grain size, Wear 296 (2012) 536–546.
[14] S. Tao, D. Li, Tribological, mechanical and electrochemical properties of nanocrystalline copper deposits produced by pulse electrodeposition, Nanotechnology 17 (2005) 65.
[15] J. Wang, J. Zhou, H. Lo`ng, Y. Xie, X. Zhang, H. Luo, Z. Deng, Q. Wei, Z. Yu, J. Zhang, Tribological, anti-corrosive properties and biocompatibility of the micro-and nano-crystalline diamond coated Ti6Al4V, Surf. Coat. Technol. 258 (2014) 1032–1038.
[16] A. Bakkar, V. Neubert, Electrodeposition and corrosion characterisation of micro-and nano-crystalline aluminium from $AlCl_3$/1-ethyl-3-methylimidazolium chloride ionic liquid, Electrochim. Acta 103 (2013) 211–218.
[17] W. Tsai, P. Hsu, Y. Hwu, C. Chen, L. Chang, J. Je, H. Lin, A. Groso, G. Margaritondo, Building on bubbles in metal electrodeposition, Nature 417 (2002) 13–19.
[18] S.M. Howdle, V.N. Bagratashvili, The effects of fluid density on the rotational Raman spectrum of hydrogen dissolved in supercritical carbon dioxide, Chem. Phys. Lett. 214 (1993) 215–219.
[19] X. Luo, C.-Y. Chen, T.-F.M. Chang, H. Hosoda, M. Sone, Crystal growth of cobalt film fabricated by electrodeposition with dense carbon dioxide, J. Electr`ochem. Soc. 162 (2015) D423–D426.
[20] G. Silvestri, S. Gambino, G. Filardo, C. Cuccia, E. Guarino, Electrochemical processes in supercritical phases, Angew. Chem. Int. Ed. Engl. 20 (1981) 101–102.
[21] J.A. Darr, M. Poliakoff, New directions in inorganic and metal-organic coordination chemistry in supercritical fluids, Chem. Rev. 99 (1999) 495–542.
[22] G.B. Jacobson, C.T. Lee, K.P. Johnston, W. Tumas, Enhanced catalyst reactivity and separations using water/carbon dioxide emulsions, J. Am. Chem. Soc. 121 (1999) 11902–11903.
[23] J. Eastoe, A. Paul, S. Nave, D.C. Steytler, B.H. Robinson, E. Rumsey, M. Thorpe, R.K. Heenan, Micellization of hydrocarbon surfactants in supercritical carbon dioxide, J. Am. Chem. Soc. 123 (2001) 988–989.
[24] S.-T. Chung, H.-C. Huang, S.-J. Pan, W.-T. Tsai, P.-Y. Lee, C.-H. Yang, M.-B. Wu, Material characterization and corrosion performance of nickel electroplated in supercritical CO_2 fluid, Corros. Sci. 50 (2008) 2614–2619.
[25] T.-F.M. Chang, M. Sone, A. Shibata, C. Ishiyama, Y. Higo, Bright nickel film deposited by supercritical carbon dioxide emulsion using additive-free Watts bath, Electrochim. Acta 55 (2010) 6469–6475.
[26] M.Z. Rahman, M. Sone, M. Eguchi, K. Ikeda, S. Miyata, T. Yamamoto, Wear properties of nickel coating film plated from emulsion with dense carbon dioxide, Surf. Coat. Technol. 201 (2006) 606–611.
[27] H. Yoshida, M. Sone, H. Wakabayashi, H. Yan, K. Abe, X.T. Tao, A. Mizushima, S. Ichihara, S. Miyata, New electroplating method of nickel in emulsion of supercritical carbon dioxide and electroplating solution to enhance uniformity and hardness of plated film, Thin Solid Films 446 (2004) 194–199.
[28] V. Nguyen, C. Lee, L. Chang, F. Chen, C. Lin, The relationship between nano crystallite structure and internal stress in Ni coatings electrodeposited by watts bath electrolyte mixed with supercritical CO_2, J. Electrochem. Soc. 159 (2012) D393–D399.
[29] L. Wang, Y. Gao, Q. Xue, H. Liu, T. Xu, Microstructure and tribological properties of electrodeposited Ni-Co alloy deposits, Appl. Surf. Sci. 242 (2005) 326–332.
[30] C. Ma, S. Wang, F. Walsh, Electrodeposition of nanocrystalline nickel-cobalt binary alloy coatings: a review, Transactions of the IMF 93 (2015) 104–112.
[31] C. Ma, Electrodeposited Nanocrystalline Ni-Co and Co-Ni-P Coatings for Hard Chromium Replacement, University of Southampton, 2013.
[32] A. Bai, C.-C. Hu, Composition controlling of Co-Ni and Fe-Co alloys using pulse-reverse electroplating through means of experimental strategies, Electrochim. Acta 50 (2005) 1335–1345.
[33] S.-T. Chung, W.-T. Tsai, Nanocrystalline Ni-C electrodeposits prepared in electrolytes containing supercritical carbon dioxide, J. Electrochem. Soc. 156 (2009) D457–D461.
[34] H.-Y. Wang, S.-T. Chung, Y.-C. Chuang, W.-T. Tsai, Electroless Ni-B deposition from an emulsified supercritical carbon dioxide bath, Thin Solid Films 518 (2010) 7505–7508.
[35] S.-T. Chung, Y.-C. Chuang, S.-Y. Chiu, W.-T. Tsai, Effect of H_3PO_3 concentration on the electrodeposition of nanocrystalline Ni-P deposited in an emulsified supercritical CO_2 bath, Electrochim. Acta 58 (2011) 571–577.
[36] S.-Y. Chiu, S.-T. Chung, C.-Y. Lin, W.-T. Tsai, Electrodeposition of Ni-Al_2O_3 composite coatings employing supercritical CO_2 baths, Surf. Coat. Technol. 247 (2014) 68–73.
[37] M.-S. Kim, J.-Y. Kim, C.K. Kim, N.-K. Kim, Study on the effect of temperature and pressure on nickel-electroplating characteristics in supercritical CO_2, Chemosphere 58 (2005) 459–465.
[38] E.D. Niemeyer, F.V. Bright, The pH within PFPE reverse micelles formed in supercritical CO_2, J. Phys. Chem. B 102 (1998) 1474–1478.
[39] H.-S. Phiong, F.P. Lucien, A.A. Adesina, Three-phase catalytic hydrogenation of α-methylstyrene in supercritical carbon dioxide, J. Supercrit. Fluids 25 (2003) 155–164.
[40] L. Devetta, A. Giovanzana, P. Canu, A. Bertucco, B. Minder, Kinetic experiments and modeling of a three-phase catalytic hydrogenation reaction in supercritical CO_2, Catal. Today 48 (1999) 337–345.
[41] A. Rashidi, A. Amadeh, The effect of saccharin addition and bath temperature on the grain size of nanocrystalline nickel coatings, Surf. Coat. Technol. 204 (2009) 353–358.
[42] B.D. Cullity, J.W. Weymouth, Elements of X-ray diffraction, Am. J. Phys. 25 (1957) 394–395.
[43] A. El-Sherik, U. Erb, J. Page, Microstructural evolution in pulse plated nickel electrodeposits, Surf. Coat. Technol. 88 (1997) 70–78.
[44] F. Czerwinski, J. Szpunar, Controlling the surface texture of nickel for high temperature oxidation inhibition, Corros. Sci. 41 (1999) 729–740.
[45] L. Chen, L. Wang, Z. Zeng, T. Xu, Influence of pulse frequency on the microstructure and wear resistance of electrodeposited Ni–Al_2O_3 composite coatings, Surf. Coat. Technol. 201 (2006) 599–605.